Aging and Disease
www.aginganddisease.org
Early access date: December 18, 2025
http://dx.doi.org/10.14336/AD.2025.1206

Original Article

A Combination of Low-Dose Δ^9-THC and Celecoxib as a Therapeutic Strategy for Alzheimer's Disease

Jian Zhang[1#], Dexiao Zhu[1#], Mei Hu[1#], Mingzhe Pan[1], Chu Chen[1*]

[1]Department of Cellular and Integrative Physiology, Joe R. and Teresa Lozano Long School of Medicine, University of Texas at San Antonio Health Science Center, San Antonio, Texas 78229, USA

[Received September 24, 2025; Revised December 2, 2025; Accepted December 3, 2025]

ABSTRACT: Alzheimer's disease (AD) is the leading cause of dementia in the elderly, and no effective therapies are currently available to prevent, treat, or halt its progression. Δ^9-Tetrahydrocannabinol (Δ^9-THC), the primary psychoactive compound in marijuana, has been considered a potential therapeutic agent, but clear evidence for its ability to prevent cognitive decline is lacking. Previous studies have demonstrated that Δ^9-THC-induced cognitive impairments are associated with the induction of cyclooxygenase-2 (COX-2). In this study, we aimed to evaluate whether Δ^9-THC alone or in combination with Celecoxib, a selective COX-2 inhibitor, could reduce neuropathology and improve cognitive function in AD model animals. We observed that Δ^9-THC (3.0 mg/kg), either alone or with Celecoxib (1.0 mg/kg), significantly reduced Aβ and tau pathologies, enhanced synaptic marker expression, and prevented the onset of cognitive decline. Notably, the combination treatment produced greater improvements in spatial learning and effectively mitigated Δ^9-THC-induced neuroinflammatory responses. Furthermore, Δ^9-THC reversed or attenuated the dysregulated expression of synaptic and immune/inflammation-related genes and restored the downregulated expression of genes linked to AD observed in both AD patients and AD animal models, with greater efficacy when combined with Celecoxib in AD model mice. These findings suggest that the combination of low-dose Δ^9-THC and Celecoxib holds promise as an early intervention strategy for preventing AD onset or treating mild cognitive impairment (MCI). Importantly, both Δ^9-THC (in the form of Dronabinol and Nabilone) and Celecoxib are FDA-approved medications already in clinical use, supporting the strong translational potential of this combination therapy and its feasibility for rapid advancement to clinical trials to assess its efficacy in preventing or delaying AD onset in humans.

Keywords: cannabis, cannabinoid, neuroinflammation, neurodegenerative disease, transcriptomics

INTRODUCTION

Alzheimer's disease (AD) is the most common cause of dementia in the elderly. Currently, more than 6.9 million people in the United States and 55 million people worldwide are living with Alzheimer's dementia, and these numbers are projected to rise to 12.7 million in the US and 153 million globally by 2050. Unfortunately, no effective therapies currently exist to prevent, treat, or halt the progression of AD. While advancing our understanding of the mechanisms underlying AD pathogenesis remains critically important, there is an urgent public health need to identify and develop novel, effective therapies for its prevention and treatment. In this context, repurposing FDA-approved drugs already in clinical use for other conditions represents a promising and efficient strategy to accelerate the development of interventions that can prevent disease onset or potentially slow or reverse AD progression.

Marijuana, or cannabis, has been used by humans for thousands of years for both recreational and medicinal purposes [1-3]. Δ^9-Tetrahydrocannabinol (Δ^9-THC) is the

***Correspondence should be addressed to:** Dr. Chu Chen, Department of Cellular and Integrative Physiology, Joe R. and Teresa Lozano Long School of Medicine, University of Texas Health Science Center at San Antonio, San Antonio, TX 78229, USA. Email: chenc7@uthscsa.edu or chen502@gmail.com. #These authors contribute equally to this work.

primary psychoactive component of marijuana. Prior laboratory studies have showed that Δ^9-THC reduces Aβ pathology both *in vitro* and *in vivo* [4-7], suggesting that Δ^9-THC may have therapeutic potential for AD [8-12]. However, the psychiatric and neurocognitive side effects associated with Δ^9-THC intoxication significantly limit its medical use and hinder research into its therapeutic potential for AD. For example, two synthetic formulations of Δ^9-THC), dronabinol (Marinol®, Syndros®) and nabilone (Cesamet®), are approved by the U.S. Food and Drug Administration (FDA) for the treatment of chemotherapy-induced nausea and vomiting in cancer patients and for managing anorexia associated with weight loss in individuals with acquired immuno-deficiency syndrome (AIDS). These synthetic analogs of Δ^9-THC have been investigated in clinical trials for the treatment of neuropsychiatric symptoms, such as agitation, in patients with AD dementia [8-12]. However, no optimal clinical dosing regimen of Δ^9-THC has been established that yields favorable outcomes in the prevention or treatment of AD [13].

In our prior work, we demonstrated that intraperitoneal co-administration of Δ^9-THC and celecoxib reduced Aβ deposition and neurodegeneration [6]. However, to date, very few studies have examined whether Δ^9-THC can improve cognitive function in AD model animals. A major challenge in advancing Δ^9-THC as a therapeutic agent for AD lies in its hormetic effects on neurocognition: high doses of Δ^9-THC (≥5.0 mg/kg) impair cognitive function [6, 14-19], whereas lower doses (≤3.0 mg/kg) have been shown to enhance learning and memory in aging animals [19, 20]. This dose-dependent variability complicates dosage optimization and clinical translation, ultimately hindering the development of effective Δ^9-THC-based therapies for both the prevention and treatment of AD. Consequently, relatively few studies, particularly those focusing on cognitive outcome, have investigated the therapeutic potential of Δ^9-THC in AD. This gap in knowledge prompted us to investigate whether Δ^9-THC can reduce Aβ and tau neuropathologies, prevent the onset of cognitive decline, and to identify the optimal dose of Δ^9-THC for reducing neuropathology and enhancing cognitive function in AD model animals.

Neuroinflammation not only drives the progression of neurodegenerative diseases but may also act as an early trigger of disease initiation [21-23]. Prior work shows that nonsteroidal anti-inflammatory drugs (NSAIDs) and selective cyclooxygenase-2 (COX-2) inhibitors can reduce inflammation and Aβ pathology in AD animal models [24-26]; however, the Alzheimer's Disease Anti-inflammatory Prevention Trial (ADAPT) and follow-ups did not demonstrate protection against incident AD or meaningful cognitive benefit [27-29], indicating that NSAIDs or COX-2 inhibitors alone are unlikely to be effective therapies for AD. While cannabinoids, including Δ^9-THC, are known to possess anti-inflammatory properties [1, 30], studies have also shown that Δ^9-THC-induced synaptic and cognitive impairments are linked to the activation of neuroinflammatory signaling pathways [6, 31-33], underscoring a dual role whereby Δ9-THC can both suppress and provoke inflammation. In particular, Δ^9-THC can activate NF-κB and COX-2, elevating cytokines and other inflammatory mediators [6, 31-33]. Pharmacological inhibition or genetic deletion of COX-2 prevents Δ^9-THC–induced memory impairments in animals [6, 31], suggesting that concurrent COX-2 inhibition, such as Celebrex (Celebrex®), may mitigate the adverse effects of Δ^9-THC on synaptic and cognitive functions, as well as its proinflammatory actions, while preserving its beneficial effects in reducing neuropathology and enhancing cognitive function in AD. In this study, we provide preclinical evidence that low-dose Δ^9-THC (3.0 mg/kg), either alone or in combination with Celecoxib (1.0 mg/kg), significantly reduced Aβ and tau neuropathologies, increased synaptic marker expression, prevented the onset of cognitive decline in AD model animals, and reversed or attenuated the dysregulated expression of AD-related genes observed in both AD patients and AD animals. Notably, the combination treatment produced more robust effects. Since both Δ^9-THC (in the form of Dronabinol and Nabilone) and Celecoxib are FDA-approved medications already in clinical use, therefore, results suggest that this combination therapy has high translational potential and could be rapidly advanced to clinical trials to evaluate its efficacy in preventing or delaying the onset of AD in humans.

MATERIALS AND METHODS

Animals

5xFAD APP transgenic (TG) mice (Stock number: 006554) and P301S (PS19) tau TG mice (Stock number: 008169) were obtained from the Jackson Laboratory, as described previously [34-37]. 5xFAD transgenic (APP-TG) mice, a widely used animal model of AD [34, 35], develop early and aggressive Aβ pathology, a key neuropathological hallmark [38]. They exhibit robust Aβ neuropathology by ~4 months and deficits in learning and memory beginning at 5 ~ 6 months [34, 35]. P301S human tau transgenic mice (PS19), a widely used tauopathy model, display progressive tau aggregation and neurofibrillary tangles with associated synaptic dysfunction, neuronal loss, and cognitive impairment, features directly relevant to the tau-driven component of AD; synaptic and cognitive impairments typically emerge ~7 months of age [36, 37]. Both male and female mice

aged five to seven months were used in this study, and animals were randomly assigned to experimental groups. All experiments were performed in a blinded fashion to prevent any scientific bias in the experiments. The experimenters were unaware of the group assignments, genotypes, or treatments, and the execution of experiments and data analysis were assigned to different individuals. The sample sizes per experimental group were estimated based on our previously published results from similar experiments and by power analysis using power=80%, α=0.05. All animal procedures were conducted in accordance with the U.S. Department of Health and Human Services Guide for the Care and Use of Laboratory Animals. The study was approved by the Institutional Animal Care and Use Committee of the University of Texas Health Science Center at San Antonio.

Δ^9-THC, with or without Celecoxib (Cel), was administered via oral gavage, a route more relevant clinical medication. The Δ^9-THC solution was prepared from a 100 mg/ml ethanol-based stock (provided by the NIH NIDA Drug Supply Program) by evaporating the ethanol under nitrogen gas. The resulting residue was resuspended in dimethyl sulfoxide (DMSO) and then sequentially diluted to 0.5 mg/mL, first in polyethylene glycol 300 (PEG300), followed by saline, resulting in a final vehicle containing 1.0% DMSO, 24% PEG300, and 75% saline. The Celecoxib (provided by the NIMH Chemical Synthesis and Drug Supply Program) was first dissolved in DMSO at a concentration of 20 mg/mL, then diluted to 0.2 mg/mL in a vehicle composed of PEG300 and saline. The same vehicle was used as the control treatment. 5xFAD mice exhibit learning and memory deficits beginning at 5~6 months [34, 35], whereas PS19 mice show synaptic and cognitive impairments around ~7 months [36, 37]. Accordingly, starting at 5 months (5xFAD) or 6 months (PS19), animals received once-daily oral gavage of vehicle (Veh), Δ^9-THC, celecoxib (Cel), or the combination (Cel + Δ9-THC) for 30 consecutive days. For preventing Δ^9-THC-triggered COX-2 upregulation, Cel was administered 30 min prior to Δ^9-THC administration in AD model animals. Δ^9-THC-only mice received a vehicle gavage at the time when Cel would have been administered, and vehicle-only mice received two vehicle gavages 30 minutes apart. The final dosing volume was adjusted according to each animal's body weight.

Reverse transcription and real-time PCR

Total RNA was extracted from harvested tissues with the RNeasy Mini Kit (Qiagen) and treated with RNase-free DNase (Qiagen), following the manufacturer's instructions. The RNA concentration was measured by a Microvolume UV-Vis Spectrophotometer (NanoDrop One, ThermoFisher Scientific), and RNA integrity was verified by electrophoresis in a 1% agarose gel. Reverse transcription was performed using the iScript cDNA synthesis kit (BioRad) with 1 µg of total RNA, with 4 µl of 5× iscript reaction mix, and 1 µl of iscript reverse transcriptase in a final volume of 20 µl. Samples were incubated at 25 °C for 5 min, followed by 42 °C for 30 min, and reactions were stopped by heating to 85 °C for 5 min.

Real-time RT-PCR primers specific for COX-1, COX-2, mPGES-1, IL-1β, IL-6, TNFα, GFAP, vimentin (Vim), and GAPDH were designed using Beacon Designer Software (BioRad) and synthesized by IDT (Coralville, IA). Primer sequences are listed in Table 1.

Table 1. List of primers used in the present study

Gene	Accession number	Forward (5'~3')	Reverse (5'~3')
β-Actin	NM_007393	TAGGCACCAGGGTGTGATGGTGGG	CGCAGCTCATTGTAGAAGGTGTGGT
IL-1β	NM_008361.33	TGGAGAGTGTGGATCCCAAGCAAT	TGTCCTGACCACTGTTGTTTCCCA
IL-6	NM_031168.1	TCTCTGGGAAATCGTGGAAATG	ACTCCAGGTAGCTATGGTACTC
TNFα	NM_013693	GTCTACTGAACTTCGGGGTGA	CACTTGGTGGTTTGCTACGAC
Vim	NM_011701	AGATGGCTCGTCACCTTCGTGAAT	TTGAGTGGGTGTCAACCAGAGGAA
GFAP	NM_010277	AACAACCTGCCTGCGTATAG	TCTCGAACTTCCTCCTCATAGAT
COX-1	BC005573	AGAAGGAGATGGCTGCTGAG	CACACGGAAGGAAACATAGGG
COX-2	BC052900	AAGCGAGGACCTGGGTTCAC	ACACCTCTCCACCAATGACCTG
mPGES-1	NM_022415	GATGAGGCTGCGGAAGAAGG	GCGAAGGCGTGGGTTCAG

Primer performance was validated using 10-fold dilutions of a mouse brain cDNA library, confirming linear amplification over five orders of magnitude with >95% efficiency. PCR products were verified by sequencing.

Reactions were performed in duplicate in a 25 µL total volume containing 12.5 µL of 2× iQ SYBR Green Supermix (Bio-Rad), 5 µL of 1:10 diluted cDNA template, and 400 nM of each primer. The PCR cycling protocol was as follows: 95 °C for 3 minutes, followed by 45 cycles of 95 °C for 30 seconds, 58 °C for 45 seconds,

and 95 °C for 1 minute. A melt-curve analysis was conducted at the end of each run to confirm amplification specificity. Amplicon sizes were further verified by electrophoresis on a 3% agarose gel. Amplification and analysis were performed using the iCycler iQ Multicolor Real-Time PCR Detection System (Bio-Rad). Relative gene expression was quantified using the $2^{-\Delta\Delta CT}$ method, with β-actin as the internal control as its expression was not affected by our experimental treatments. ΔCT was calculated as (CT of gene of interest) - (CT of β-actin), and ΔΔCT as (ΔCT of treated sample) - (ΔCT of control), as previously described [39, 40]. Technical replicates were performed for each detected gene to ensure measurement accuracy and reproducibility.

Single-nucleus RNA sequencing sample preparation, library construction, and sequencing

Sample preparation, library construction, and RNA sequencing

Hippocampal tissues from WT, APP-TG mice treated with Veh, Δ^9-THC, Cel, and Δ^9-THC + Cel for single-nucleus RNA sequencing were harvested and stored in liquid nitrogen as previously described [41, 42]. Single nucleus sample preparation, library construction, and RNA sequencing were outsourced to Novogene Corporation Inc. (Sacramento, CA). Single nucleus RNA sequencing libraries were prepared using the Chromium Next GEM Single Cell 3′ Gel Bead Kit (Dual Index) v.3.1 (10x Genomics) and sequencing was performed on the Illumina NovaSeq6000 system at Novogene.

RNA-Seq Data Processing and Analysis

Sequencing data were processed using Cell Ranger (v4.0) and analyzed with Seurat (v5.2.1) in R (v4.3.3). Before downstream analysis, sequencing data were processed with CellBender (v0.2.0) to remove ambient RNA. Low-quality nuclei were removed based on quality thresholds: <30% mitochondrial. Genes expressed in fewer than 10 nuclei were excluded. Nuclei were retained if they expressed between 400 and 6,000 genes and had ≤35,000 UMIs. For doublet or multiplet detection, we carefully examined the expression of canonical cell type–specific marker genes within each cluster. Clusters that simultaneously expressed markers from multiple distinct cell types were considered potential doublet or multiplet clusters and were subsequently excluded from downstream analyses.

Normalization was performed using a scale factor of 10,000, and 3,000 highly variable genes were identified using the 'vst' method. Principal component analysis (PCA) was conducted using the top 30 components. Clustering was performed at a resolution of 2, and dimensionality reduction was visualized with tSNE. Integrated analysis of snRNA-seq data was performed to remove mismatched clusters (e.g., neuronal markers detected in non-neuronal snRNA-seq data); default batch-effect correction in Seurat was applied to datasets.

Cell-Type Annotation

Mouse hippocampal cell types were annotated manually using established gene markers as listed in Supplementary Figure 1B. For human hippocampal samples from previously published literature [43], we used the following markers: CA1 pyramidal neurons: *syt1*, *mpped1*, and *pex5l*; CA3 pyramidal neurons: *syt1*, *prkcb*, and *cpne4*; dentate gyrus granule cells: *syt1*, *prox1*, and *stxbp6*; inhibitory neurons: *syt1*, *gad1*, and *gad2*; astrocytes: *aqp4* and *slc1a2*; microglia: *cd74* and *csf1r*; oligodendrocytes: *plp1* and *mbp*; oligodendrocytes precursor cells*: pdgfra*.

Differential Gene Expression and Functional Analysis

Differentially expressed genes (DEGs) were identified using Seurat's FindMarkers function with the Wilcoxon rank-sum test. DEGs were defined by a P value < 0.01 and absolute $\log_2$ fold-change > 0.5. Synaptic genes were further filtered using the SYNGO databases. AD risk genes were downloaded from KEGG database, and ID is *mmu05010*. We also add some genes from previous studies manually. Immune and inflammation related genes were collected from previous studies. Data visualization—including heatmaps, volcano plots, and violin plots—was performed using Seurat and OriginLab 2024. In the heatmaps of avg_$\log_2$FC values, cells with NA values were displayed in white. Normalized expression values used in heatmaps were produced by modified jjDotPlot function scRNAtoolVis package (see data available). GO analyses were generated via ClusterProfiler (version 4.10.1) and Org.Mm.eg.db (version 3.18.0) with default parameters.

Cell-Cell Communication Analysis

Cell-cell communication was assessed using the CellChat package (v2.1.2) in R (v4.3.3), following the standard workflow outlined in the package guidelines [44]. Preprocessed single-cell RNA-seq data, previously analyzed using Seurat, were imported into CellChat for downstream interaction analysis.

Gene Regulatory Network Analysis

We applied (pySCENIC [45] at https://pyscenic.readthedocs.io) to a subset of cells from our dataset to infer gene regulatory networks (GRNs). Initial GRN construction was guided by a comprehensive list of transcription factors from https://github.com/aertslab (file name is mm_mgi_tfs.txt). These networks were subsequently refined to retain only downstream target genes with predicted transcription factor binding motifs located within 5 kb of the transcription start site (TSS). Next, area under the curve (AUC) scores were computed for each regulon across cells, followed by z-score normalization. A regulon was considered expressed within a cell type if its average z-scored AUC exceeded zero. To assess differences in regulon activity across experimental conditions: WT-Veh, APP-TG-Veh, APP-TG-THC, APP-TG-Cel, and APP-TG-Cel-THC, the z-scored AUC values of expressed regulons were compared using one-way ANOVA, and P values were calculated accordingly.

Immunoblot

Western blot assays were performed to assess the expression of APP, BACE1, nicastrin (NCT), neprilysin (NEP), $A\beta_{42}$, total tau (Tau-5), phosphorylated tau (p-Tau181), AT8 (p-Tau S202/T205), glutamate receptor subunits (GluA1, GluA2, GluN1, GluN2A, and GluN2B), and PSD-95 in hippocampal tissues from WT, 5xFAD (APP-TG), or PS19 (tau-TG) mice, as previously described [41, 46].

Tissues were extracted and immediately homogenized in RIPA lysis buffer containing protease inhibitors, incubated on ice for 30 minutes, and centrifuged at 10,000 rpm for 10 minutes at 4 °C. Supernatants were separated on 4-15% SDS-PAGE gels (Bio-Rad) and transferred onto PVDF membranes (Bio-Rad). Membranes were incubated overnight at 4 °C with primary antibodies (listed in Table 2), then washed and incubated with a secondary antibody (goat anti-rabbit, 1:2,000; Cell Signaling) for 1 hour at room temperature.

Table 2. List of antibodies used in the present study.

Antibody	Ratio (WB)	Ratio (IHC)	Manufacture	Cat#	RRID
BACE1	1:1,000		Abcam	ab108394; 617C17C-100	AB_10861218
APP	1:1,000	1:200	MilliporeSigma	A8717	AB_258409
4G8		1:2,000	BioLegend	SIG-39220-200	AB_662812
NCT	1:1,000		Cell Signaling	5665	AB_10694688
Neprilysin	1:500		Novus	NBP2-15771	AB_3263106
Aβ42	1:1,000		Thermos Fisher	44-344	AB_2313572
GluA1	1:1,000		Abcam	ab31232	AB_2113447
GluA2	1:1,000		Abcam	ab133477	AB_2620181
GluN1	1:500		Abcam	ab109182	AB_10862307
GluN2A	1:1,000		MilliporeSigma	07-632	AB_310837
GluN2B	1:1,000		Abcam	ab65783	AB_1658870
PSD-95	1:1,000		Abcam	Ab2723	AB_303248
p-tau-T181	1:1,000	1:500	Cell Signaling	12885	AB_2798053
Tau-5	1:1,000		Thermos Fisher	AHB0042	AB_2536235
AT8	1:1,000		Thermos Fisher	MN1020	AB_223647
GFAP	1:1,000	1:500	MilliporeSigma	G3893	AB_477010
Iba-1		1:200	MilliporeSigma	MABN92	AB_10917271
β-Actin	1:2,000		Santa Cruz	Sc-47778	AB_626632

Proteins were visualized using enhanced chemiluminescence (ECL; Amersham Biosciences, UK), and band intensities were quantified by densitometry using the GE/Amersham Imager 680 UV. Band densities were normalized to total protein loading using mouse anti-β-actin (1:2,000; Santa Cruz), as previously described [41, 46].

ELISA

Whole hippocampi were lysed to generate total protein extracts. Tissues were homogenized in the lysis buffers supplied with the respective ELISA kits, including Aβ42 (AnaSpec, Inc.), IL-1β (MyBioSource) and TNFα (MilliporeSigma), and all procedures followed the manufacturers' instructions [46, 47]. Each kit included calibration (standard) curves, which we used to calculate absolute protein concentrations. Pilot experiments were performed to optimize loading volumes and ensure all measurements fell within the linear range of the standard curves. Absorbance was measured on a SpectraMax® iD3 plate reader (Molecular Devices). The same animals were used for both Western blot (WB) and ELISA analyses to enable direct comparison across methods and to minimize inter-animal variability. Technical replicates were

performed for each detected protein to ensure accuracy and reproducibility.

Immunofluorescence and histochemistry

Immunofluorescence analysis was performed to assess Aβ, Iba1 and GFAP in coronal brain sections. Animals were anesthetized with ketamine/xylazine (200/10 mg/kg) and subsequently transcardially perfused with PBS followed by 4% paraformaldehyde in phosphate buffer. The brains were quickly removed from the skulls and fixed in 4% paraformaldehyde overnight and then transferred into the PBS containing 30% sucrose until sinking to the bottom of the small glass jars. Cryostat sectioning was made on a freezing Vibratome at 30 μm and a series 5 to 8 equally spaced (every 10 sections) sections were collected in 0.1M phosphate buffer. Free floating sections were immunostained using specific antibodies as listed in Supplemental Table 2 and followed by incubation with the corresponding fluorescent-labeled secondary antibody. 4′-6-Diamidino-2-phenylindole (DAPI), a fluorescent stain that binds strongly to DNA, was used to detect cell nuclei in the sections. The sections were then mounted on slides for immunofluorescence imaging. Imaging was performed on a Zeiss Axio Imager 2 deconvolution microscope. Brain regions of interest (ROIs) were defined using standard cytoarchitectural landmarks and included cortex, CA1, and dentate gyrus (DG). Immunostaining data were acquired and analyzed in SlideBook 6.0 (Intelligent Imaging Innovations, Denver, CO). Acquisition settings (exposure time and γ) were held constant across groups, and background was subtracted uniformly as described previously [35, 41, 46, 47]. Thresholds for morphology-based segmentation were determined from channel histograms using SlideBook's built-in algorithms to distinguish signal from background. For each image, the antibody-specific channel within the ROI was quantified in arbitrary densitometric units (ADU). Values were normalized to the vehicle control group, as described previously [41, 46].

Degenerating neurons were detected using Fluoro-Jade C (FJC), an anionic dye that specifically stains the soma and neurites of degenerating neurons, making it a unique marker for neurodegeneration. Cryostat-cut sections were incubated for 10 minutes in a solution containing FJC (0.0001%, EMD Millipore) and DAPI (0.5 μg/mL), followed by three 1-minute washes with distilled water. Sections were then air-dried at room temperature in the dark. FJC-positive cells in the cortex and hippocampus were imaged and analyzed using a Zeiss deconvolution microscope with SlideBook 2024 software, as previously described. [35, 41].

Behavioral tests

Novel object recognition test

The novel object recognition (NOR) test was performed to assess memory retention as described previously [36, 46, 48-50]. Briefly, the NOR test was conducted in a 30 × 30 × 30 cm square open field. Mice first underwent a 10-minute habituation session in the empty arena. The NOR assay then comprised two 10-minute stages separated by a 4-hour intertrial interval. In the training stage, animals were presented with two identical objects. In the test stage, animals were presented with one familiar object (from training) and one novel object. Exploration was defined as the time spent with the head oriented toward and within 2 cm of an object. Object exploration during the test stage was quantified using the EthoVision video-tracking system (Noldus). The recognition index (RI) was calculated based on the following equation: $RI = T_N/T_N+T_F$), where T_N is the exploration time devoted to the novel object and T_F is the exploration time for the familiar object, as described previously [46, 49].

Morris water Maze test

The classic Morris water maze (MWM) test was used to determine spatial learning and memory, as described previously [6, 35, 36, 41, 47, 48, 51]. Briefly, a circular water tank (diameter 120 cm and 75 cm in high) was filled with water, and the water was made opaque with non-toxic white paint. A round platform (diameter 15 cm) was hidden 1 cm beneath the surface of the water at the center of a given quadrant of the water tank. WT, APP TG, and tau-TG mice treated with WT-Veh, APP-TG-Veh, APP-TG-THC, APP-TG-Cel, and APP-TG-Cel-THC received learning acquisition training in the Morris water maze for 7 days and each session consisted of 4 trials. For each trial, the mouse was released from the wall of the tank and allowed to search, find, and stand on the platform for 5 seconds within the 60-second trial period. For each training session, the starting quadrant and sequence of the four quadrants from where the mouse was released into the water tank were randomly chosen so that it was different among the separate sessions for each animal and was different for individual animals. The mouse movement in the water pool was recorded by a video-camera and the task performances, including swimming paths, speed, and time spent in each quadrant were recorded using an EthoVision video tracking system (Noldus). A probe test was conducted 24 h after the final acquisition session. For the probe test, the platform was removed, and behavior was recorded for 60 seconds. Memory retention was assessed by (1) time spent in the target quadrant and (2) the number of crossings over the

former platform location. Behavior was recorded and analyzed automatically using EthoVision XT. No animals were excluded unless they exhibited motor impairments, excessive floating (>50% of the trial duration), or visible health issues; no mice met these criteria in the present study.

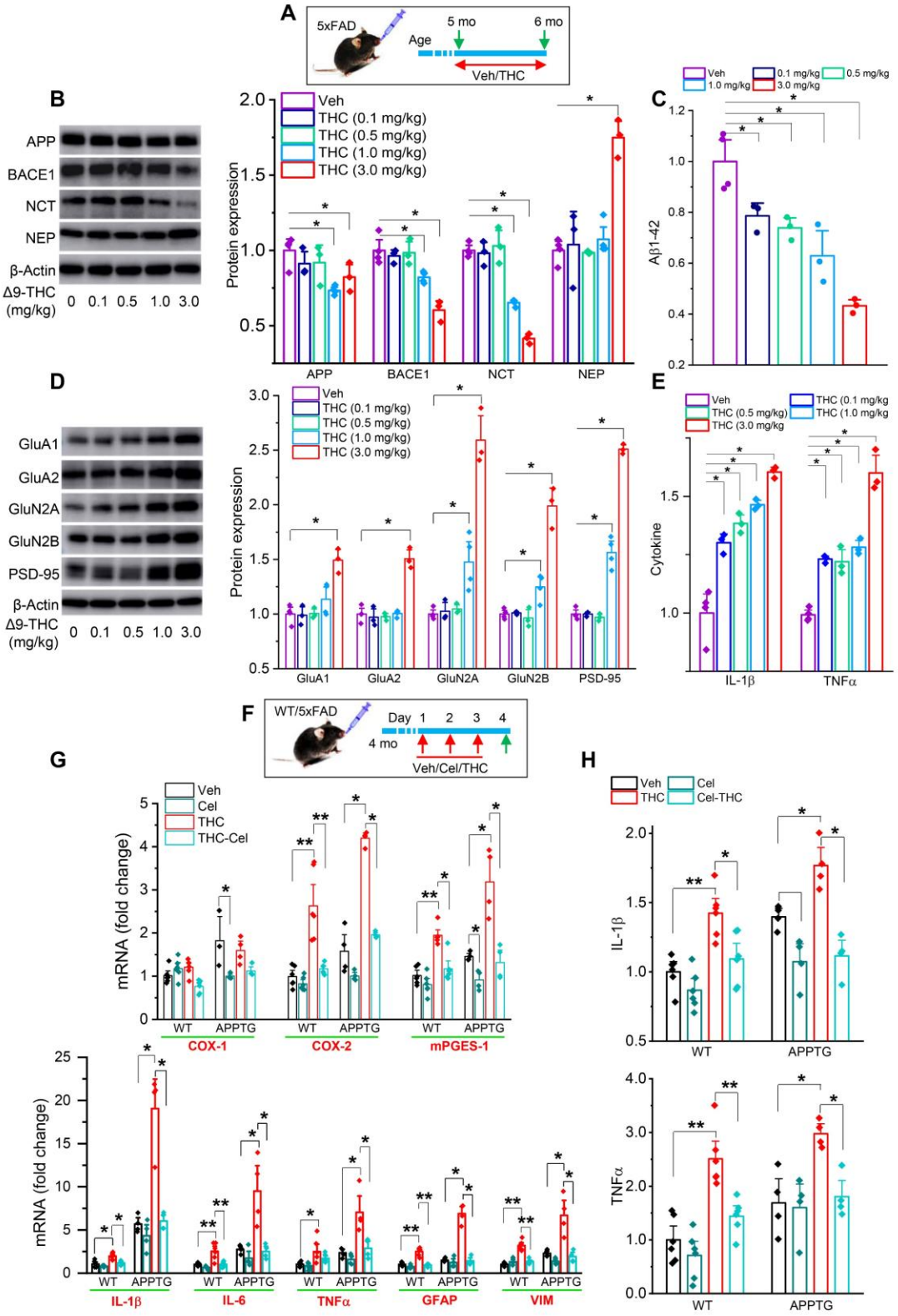

Figure 1. Optimize Δ^9-THC dosing for Δ^9-THC intervention. (A) Schematic illustration of the Δ^9-THC dosing protocol. 5xFAD APP-TG mice at five months of age received different doses of Δ^9-THC, and Aβ pathology along with the expression of synaptic markers was assessed after 30 days. **(B)** Expression of amyloid precursor protein (APP) and Aβ processing enzymes, including BACE1, nicastrin (NCT, a component of γ-secretase complex), and neprilysin (NEP) in the hippocampus of APP-TG mice treated with varying doses of Δ^9-THC. Data are presented as means ±SEM. *P=0.0339 (Mann-Whitney test, Veh and THC-1.0 mg: n=4 animals/group; the rest groups: n=3 animals/per group). **(C)** ELISA analysis of Aβ42 levels in hippocampal tissues of APP-TG mice treated with Δ^9-THC. Data are presented as means ±SEM. * P=0.0339 (Mann-Whitney test, Veh: n=4 animals/group; THC: n=3 animals/per group). **(D)** Immunoblot analysis of synaptic marker expression, including PSD-95 and glutamate receptor subunits (GluA1, GluA2, GluN2A and GluN2B), in hippocampal tissues of APP-TG mice treated with Δ^9-THC. Data are presented as means ±SEM. *P=0.0339 (Mann-Whitney test, Veh and THC-1.0 mg: n=4 animals/group; the rest groups: n=3 animals/per group). **(E)** ELISA analysis of cytokine levels, including IL-1β and TNFα, in hippocampal tissues of APP-TG mice treated with Δ^9-THC. Data are presented as means ±SEM. *P=0.0339 (Mann-Whitney test, Veh: n=4 animals/per group; THC: n=3 animals/per group). **(F)** Schematic illustration of the experimental protocol for combination treatment with Δ^9-THC, with or without Celecoxib (Cel) in both WT and APP- TG mice. **(G)** qPCR analysis of inflammatory marker expression, including cyclooxygenase 1 (COX-1), COX-2, microsomal prostaglandin E synthase-1 (mPGES-1), IL-1β, IL-6, TNFα, GFAP, and vimentin (VIM), in hippocampal tissues of WT and APP-TG mice treated with Δ^9-THC or Cel. Data are presented as means ±SEM. *p=0.0286, **p=0.0130 (Kruskal-Wallis test followed by Dunn's post hoc test with Bonferroni correction for comparisons; WT: n=6 animals/per group, APP-TG: n=4 animals/per group). **(H)** ELISA analysis of cytokine levels, including IL-1β and TNFα, in hippocampal tissues of WT and APP-TG mice treated with Δ^9-THC or with Cel. Data are presented as means ±SEM. *p=0.0286, **p=0.0130 (Kruskal-Wallis test followed by Dunn's post hoc with Bonferroni correction for comparisons; WT: n=6 animals/per group, APP-TG: n=4 animals/per group).

Data analysis

Data are presented as mean ± S.E.M. Statistical analyses were performed using StatView and GraphPad Prism. Unless stated otherwise, parametric tests (*e.g.,* one- or two-way ANOVA with appropriate post hoc comparisons) were applied when normality assumptions were met. Non-parametric alternatives were used (*e.g.*, Mann-Whitney for two groups; Kruskal-Wallis followed by Dunn's tests for multiple group comparisons) when group sizes were <6. Exact *p* values and the number of observations (*n*) for each group are indicated in the figures or reported in the corresponding figure legends.

RESULTS

Determining the optimal dose of Δ^9-THC for AD therapy

Previous research has revealed that Δ^9-THC doses higher than 5.0 mg/kg impair cognition, while doses of 3.0 mg/kg or lower enhance memory in aging animals [6, 14-17, 20, 52]. To avoid the severe neuropsychiatric and cognitive impairments associated with high doses, we selected a dose range of 0.1 to 3.0 mg/kg to determine the optimal dose for AD therapy. We evaluated this range by assessing Aβ pathology and synaptic markers in the hippocampus of 5xFAD transgenic (APP-TG) mice, a widely used animal model of AD [34, 35], as Aβ pathology is one of the key neuropathology hallmarks and early-stage AD is characterized by synaptic dysfunction [38]. These mice exhibit robust Aβ neuropathology at 4 months of age and deficits in learning and memory beginning at 5 ~ 6 months of age [34, 35]. Therefore, we administered Δ^9-THC via oral gavage, a route that is more relevant clinical medication, starting at 5 months of age, once daily for 30 days (Fig. 1A). As shown in Fig.1B, Δ^9-THC at doses of 0.1 and 0.5 mg/kg dis not alter the expression of β-amyloid precursor protein (APP), β-site amyloid precursor protein cleaving enzyme 1 (BACE1), or nicastrin (NCT), enzymes involved in Aβ synthesis, nor did it affect neprilysin (NEP), the enzyme responsible for Aβ degradation. However, at 1.0 mg/kg, Δ^9-THC significantly reduces APP, BACE1 and NCT levels, suggesting that this dose may be the minimal effective dosage in reducing Aβ pathology in APP-TG mice. Notably, at 3.0 mg/kg, Δ^9-THC induced a robust reduction in APP, BACE1 and NCT, while also increasing NEP expression. ELISA analysis further revealed a dose-dependent decrease in soluble Aβ42 levels, with a reduction of more than 50% observed at 3.0 mg/kg (Fig. 1C). Similarly, we did not observe significant changes in the expression of glutamate AMPA and NMDA receptor subunits or PSD-95 at doses of 0.1, 0.5, 1.0 mg/kg (Fig. 1D). However, at 3.0 mg/kg, Δ^9-THC significantly increased all assessed synaptic markers. These results suggest that Δ^9-THC at 3.0 mg/kg is likely the optimal dose for maximizing the reduction of Aβ pathology and improving synaptic integrity while avoiding the detrimental cognitive effects observed at higher doses.

To further validate that Δ^9-THC at 3.0 mg/kg is the optimal dose for reducing neuropathology and enhancing synaptic function, we conducted an additional set of experiments. As shown in Fig. 2, Δ^9-THC at 3.0 mg/kg significantly reduced Aβ pathology (Fig. 2A), increased the expression of synaptic markers (Fig. 2B), and attenuated neurodegeneration (Fig. 2C).

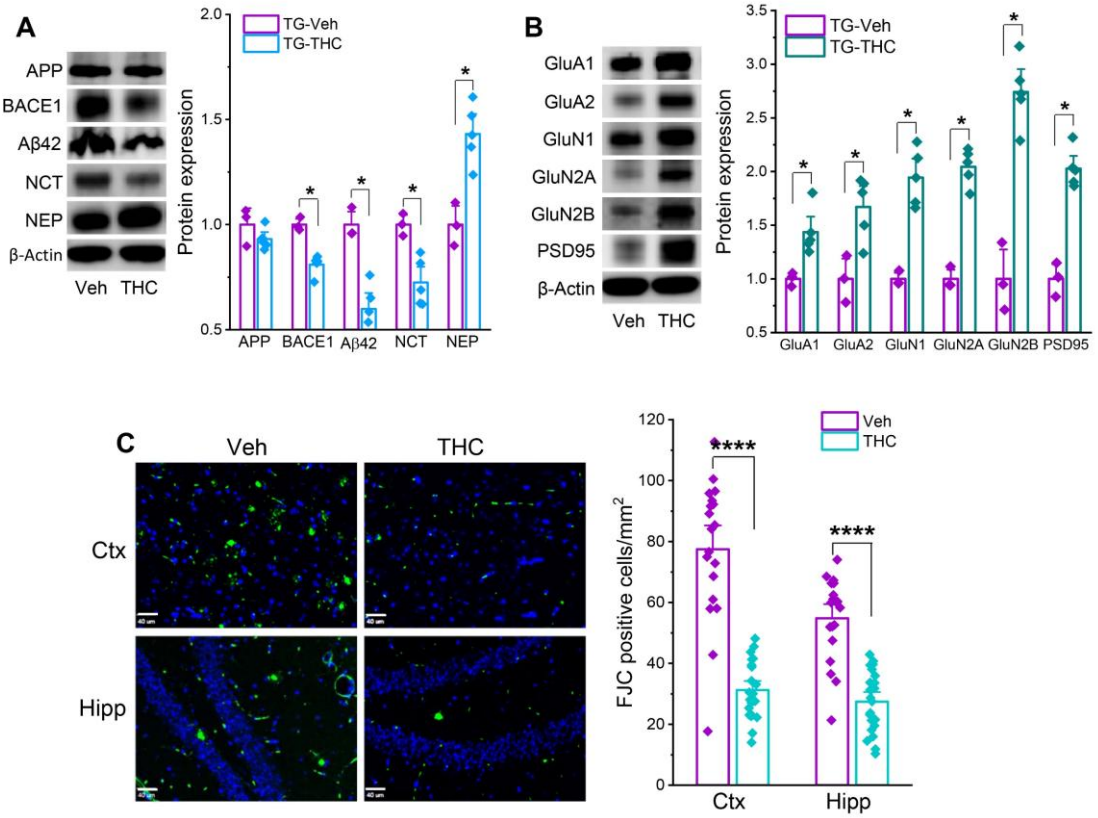

Figure 2. Δ^9-THC reduces Aβ pathology, neurodegeneration and enhances synaptic marker expression in 6-month-old 5xFAD mice. Δ^9-THC (3.0 mg/kg) was administered via oral gavage in 5xFAD APP-TG mice at 5 months of age. Assessments were performed 30 days after last administration. **(A)** Immunoblot analysis of hippocampal expression of APP, BACE1, NCT, NEP, and Aβ42 in APP-TG mice treated with vehicle or Δ^9-THC. Data are presented as means ±SEM. *p=0.0253 (Mann-Whitney test, Veh: n=3 animals/group; THC: n=5 animals/per group). **(B)** Immunoblot analysis of synaptic marker expression, including PSD-95 and glutamate receptor subunits (GluA1, GluA2, GluN1, GluN2A and GluN2B), in hippocampal tissues of APP-TG mice treated with Δ^9-THC. Data are presented as means ±SEM. *p=0.0253 (Mann-Whitney test, Veh: n=3 animals/group; THC: n=5 animals/per group). **(C)** Fluoro-Jade C (FJC) staining of degenerating neurons in the Ctx and Hipp of APP-TG mice treated with Δ^9-THC. Data are presented as means ±SEM. ****P<0.0001 (ANOVA with Bonferroni post-hoc test, 19 images for Veh and 22 images for THC, n=5 animals per group). Scale bars: 40 μm.

Previous research has shown that higher doses of Δ^9-THC (8 and 10 mg/kg) activate neuroinflammatory COX-2 and NF-kB signaling pathways, resulting in increased cytokine production and elevated expression and activity of COX-2 and its downstream derivatives, such as prostaglandins [6, 31-33]. Given the detrimental effects of neuroinflammation on brain function, we assessed cytokine levels to determine whether lower doses of Δ^9-THC also trigger inflammatory responses in 5xFAD APP-TG mice. Our results revealed that even at a lower dose (0.1 mg/kg), Δ^9-THC significantly increased the production of IL-1β and TNF-α (Fig. 1E). As 3.0 mg/kg was identified as the optimal dose of Δ^9-THC for AD, we further investigated whether the Δ^9-THC-induced increase in inflammatory markers at this dose could be mitigated by Celecoxib (Cel), a selective COX-2 inhibitor, at an extremely low dose of 1.0 mg/kg. Four-month-old WT and APP-TG mice were treated with vehicle (Veh), Cel, Δ^9-THC, or Cel + Δ^9-THC once daily for three days, and assays were performed one day after the final oral gavage dose (Fig. 1F). As shown in Fig. 1G, Δ^9-THC (3.0 mg/kg) significantly increased the mRNA expression of inflammatory markers, including COX-2, microsomal prostaglandin E synthase-1 (mPGES-1), IL-1β, IL-6, TNF-α, glial fibrillary acidic protein (GFAP), and vimentin (VIM) in the hippocampus of both WT and APP-TG mice, with more robust increases observed in APP-TG mice compared to WT animals. However, these increases were significantly attenuated by Cel treatment. Both ELISA and immunoblot analyses further demonstrated that Δ^9-THC-induced increases in the expression IL-1β and TNF-α were inhibited by Cel (Fig. 1H).

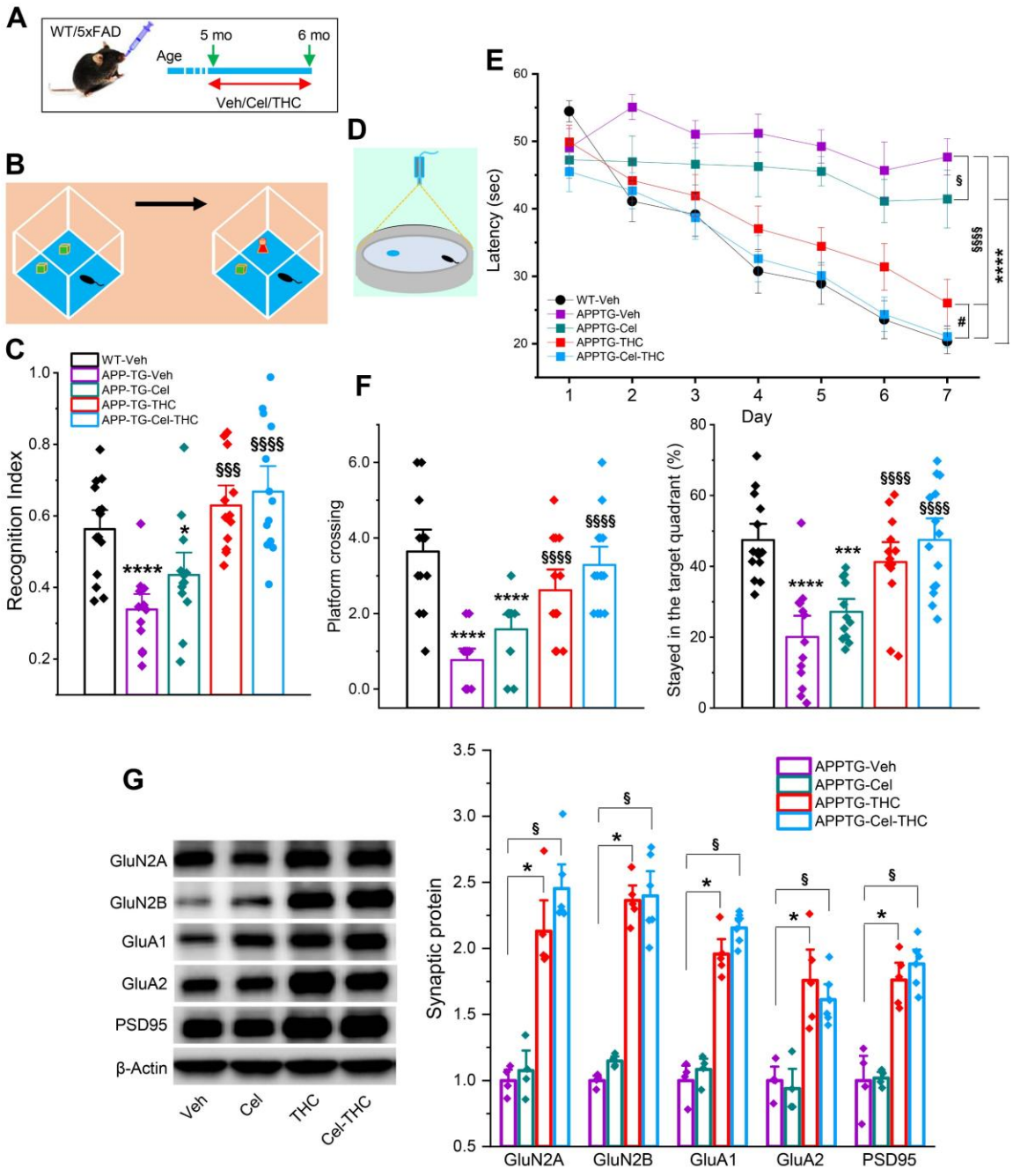

Figure 3. Δ^9-THC, alone or in combination with Celecoxib, improves cognitive function and preserves synaptic integrity in APP-TG mice. (A) Schematic illustration of the experimental protocol for treatment with Δ^9-THC, with or without Celecoxib (Cel), in 5xFAD APP-TG mice. **(B)** Cartoon illustration of the novel object recognition (NOR) test. **(C)** Memory retention was assessed using the NOR test in APP TG mice treated with Δ^9-THC, with or without Cel. Data are presented as means ± SEM. *P= 0.0230, ****P< 0.0001 vs WT-Veh, §§§P=0.0012, §§§§P< 0.0001 vs APP-TG-Veh (ANOVA with Bonferroni post hoc test, WT-Veh: n =14 animals per group, APP-TG-Veh: n=13 animals per group, APP-TG-Cel: n =13 animals per group, APP-TG-THC: n =12 animals per group, APP-TG-Cel-THC: n =14 animals per group). **(D)** Illustration of the Morris water maze (MWM) test. **(E)** Spatial learning and memory were assessed using the MWM test in APP TG mice treated with Δ^9-THC, with or without Cel. Data are presented as means ± SEM. ****P < 0.0001 vs WT-Veh; §P=0.0341, §§§§P< 0.0001vs APP-TG-Veh; #P=0.0501 vs APP-TG-THC (Repeated measures ANOVA with Bonferroni post hoc test, WT-Veh: n =14 animals per group, APP-TG-Veh: n=13 animals per group, APP-TG-Cel: n =12 animals per group, APP-TG-THC: n =13 animals per group, APP-TG-Cel-THC: n =14 animals per group). **(F)** The probe test was conducted 24 hours following 7 days of learning acquisition training. Data are presented as means ± SEM. ***P=0.0002, ****P <

0.0001 vs WT-Veh; §§§§P< 0.0001vs APP-TG-Veh (ANOVA with Bonferroni post hoc test). **(G)** Immunoblot analysis of synaptic marker expressions in APP TG mice with Δ^9-THC, with or without Cel. Data are presented as means ±SEM. *p=0.0480, §p=0.0286 (Kruskal-Wallis test followed by Dunn's post hoc test with Bonferroni correction for comparisons; Veh: n=4 animals/per group, Cel: n=4 animals/per group, THC: n=5 animals/per group, Cel-THC: n=6 animals/per group).

The data presented above indicate that Δ^9-THC at 3.0 mg/kg effectively reduces Aβ pathology and increases expression of synaptic markers, while Δ^9-THC-induced inflammatory responses can be mitigated by concurrent administration of Cel at 1.0 mg/kg in APP-TG mice. Therefore, we selected 3.0 mg/kg Δ^9-THC (human equivalent doses: 0.24 mg/kg) in combination with 1.0 mg/kg Cel (human equivalent doses: 0.08 mg/kg) as the optimal regimen to evaluate the efficacy of this combination in alleviating neuropathology and improving neurocognitive function in AD model mice.

Δ^9-THC alone or in combination with Cel improves learning, memory, and synaptic integrity in APP-TG mice

Amnesia, or memory loss, is a hallmark symptom of AD. Therefore, we first assessed whether Δ^9-THC or its combination with Cel could enhance learning and memory or prevent the disease onset in AD model animals. APP-TG mice at five months of age were treated with Veh, Cel, Δ^9-THC, or Cel + Δ^9-THC once daily for 30 days (Fig. 3A). Memory retention in these mice was evaluated using the novel object recognition (NOR) test (Fig. 3B). As expected, vehicle-treated APP-TG mice at six months of age exhibited impaired memory retention compared with WT controls (Fig. 3C). While Cel alone did not significantly improve NOR performance, treatment with Δ^9-THC or the combination of Cel + Δ^9-THC effectively prevented or rescued memory deficits in APP-TG mice. These findings suggest that Δ^9-THC, either alone or in combination with Cel enhances memory in AD animals.

These findings were further confirmed using the Morris water maze (MWM) test (Fig. 3D). As shown in Fig. 3E~F, Δ^9-THC alone or in combination with Cel significantly improved spatial learning and memory retention in APP-TG mice. Notably, APP-TG mice treated with Cel + Δ^9-THC displayed better spatial learning performance compared to those treated with Δ^9-THC alone (Fig. 3E). Additionally, Cel slightly enhanced spatial learning in APP-TG mice. To further investigate the effects of Δ^9-THC or its combination with Cel on synaptic integrity, we assessed the expression of key synaptic markers involved in synaptic transmission and plasticity. Our previous study demonstrated that the expression of glutamate AMPA receptor subunits (GluA1 and GluA2), NMDA receptor subunits (GluN2A and GluN2B), and PSD-95 is significantly reduced in 6-month-old 5xFAD mice [35]. Here, we found that the reduced expression of these synaptic markers was robustly restored by Δ^9-THC alone or Cel + Δ^9-THC (Fig. 3G). These data indicate that Δ^9-THC, either alone or in combination with Cel, enhances synaptic and cognitive functions and prevents cognitive decline in AD animals.

Δ^9-THC alone or in combination with Cel reduces neuroinflammation and neuropathology in APP-TG mice

Neuroinflammation is widely recognized as a key contributor in the development of neurodegenerative diseases [21-23]. Additionally, Δ^9-THC has been shown to activate neuroinflammatory signaling pathways, leading to elevated levels of cytokines, COX-2, and other inflammatory factors [6, 31-33]. Astrogliosis is widely recognized as a hallmark of neuroinflammation in neurodegenerative diseases. To assess whether Δ^9-THC increases astrocyte and microglial reactivity, and whether this effect can be attenuated by Cel, we examined the immunoreactivity of GFAP (an astrocytic marker) and Iba1 (a microglial marker) in APP-TG mice. As shown in Fig. 4B~C, GFAP and Iba1 immunoreactivity was increased in APP-TG mice when compared with WT. Cel alone reduced gliosis in APP-TG mice. In contrast, Δ^9-THC alone further increased GFAP and Iba1 immunoreactivity, indicating heightened astrocyte and microglial activation. However, this Δ^9-THC-induced gliosis was effectively attenuated by co-administration of Cel in APP-TG mice. These findings suggest that while Δ^9-THC exacerbates neuroinflammation, COX-2 inhibition with Cel effectively mitigates this effect in APP-TG mice.

Next, we examined Aβ pathology and found that both Δ^9-THC alone and the combination of Cel + Δ^9-THC significantly reduced BACE1, NCT, Aβ42, and Aβ plaque deposition while increasing NEP levels (Fig. 4D~E). These results indicate that Δ^9-THC reduces Aβ pathology not only by suppressing Aβ synthesis enzymes but also by enhancing Aβ clearance mechanisms. Neurodegeneration is a hallmark of AD neuropathology. Using Fluoro-Jade C (FJC), a marker for degenerating neurons, we found that both Δ^9-THC alone and the combination of Cel + Δ^9-THC significantly reduced the number of FJC-positive neurons in 6-month-old APP-TG mice (Fig. 4F). These data indicate that Δ^9-THC, either alone or in combination with Cel, reduces AD neuropathology and that co-administration with Cel attenuates Δ^9-THC-induced exacerbation of neuroinflammation in APP-TG mice.

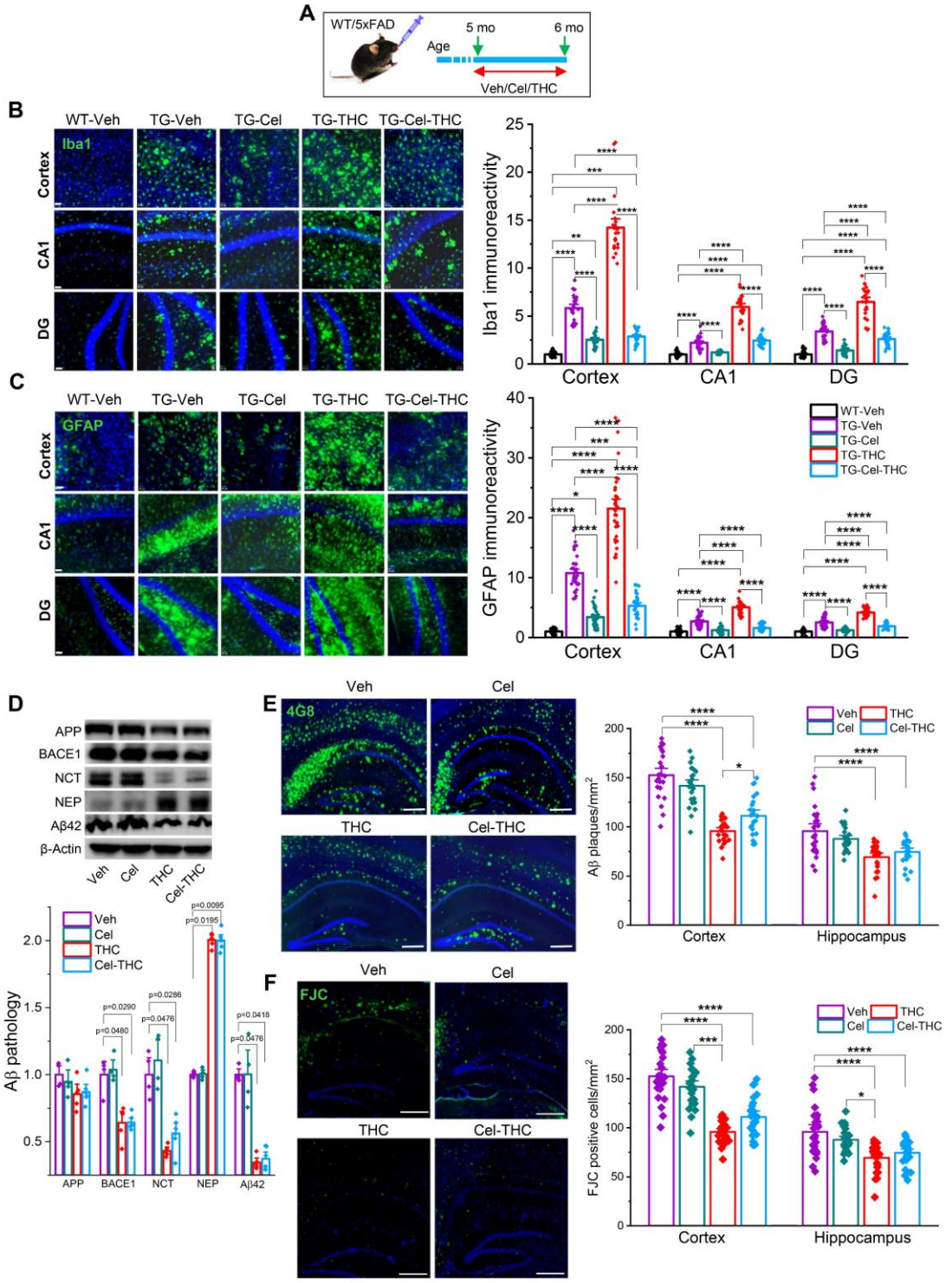

Figure 4. The combination treatment reduces neuropathology and Δ⁹-THC-induced glial cell reactivity. (A) Schematic illustration of the experimental protocol. **(B)** Immunostaining analysis of Iba1 immunoreactivity in the brain of APP-TG mice treated with Δ⁹-THC, with or without Cel. Data are presented as means ±SEM. **p=0.0042, ***p=0.0005, ****p<0.0001 (ANOVA with Bonferroni post-hoc test, WT-Veh: 27 images/5 animals, APP-TG-Veh: 28 images/6 animals, APP-TG-Cel: 24 images/5 animals, APP-TG-THC: 25 images/5 animals, APP-TG-THC: 28 images/6 animals). Scale bars: 40 μm. **(C)** Immunostaining analysis of GFAP immunoreactivity in the brain of APP-TG mice treated with Δ⁹-THC, with or without Cel. Data are presented as means ±SEM. *p=0.0275, ***p=0.0005, ****p<0.0001 (ANOVA with Bonferroni post-hoc test, WT-Veh: 35 images/5 animals, APP-TG-Veh: 37 images/6

animals, APP-TG-Cel: 34 images/5 animals, APP-TG-THC: 35 images/5 animals, APP-TG-THC: 34 images/6 animals). Scale bars: 40 μm. **(D)** Immunoblot analysis of APP, Aβ42, and Aβ processing enzymes, including BACE1, NCT, and NEP in hippocampal tissues of APP-TG mice treated with Δ^9-THC, with or without Cel. Data are presented as means ±SEM (Kruskal-Wallis test followed by Dunn's post hoc test with Bonferroni correction for comparisons; Veh: n=4 animals/per group, Cel: n=4 animals/per group, THC: n=5 animals/per group, Cel-THC: n=6 animals/per group). **(E)** Immunostaining analysis of 4G8 (total Aβ) immunoreactivity in the cortex (Ctx) and hippocampus (Hipp) of APP-TG mice treated with Δ^9-THC, with or without Cel. Data are presented as means ±SEM. *p=0.0341, ****p<0.0001 (ANOVA with Bonferroni post-hoc test, APP-TG-Veh: 25 images/5 animals, APP-TG-Cel: 25 images/5 animals, APP-TG-THC: 25 images/5 animals, APP-TG-THC: 24 images/5 animals). Scale bars: 400 μm. **(F)** Fluoro-Jade C (FJC) staining of degenerating neurons in the Ctx and Hipp of APP-TG mice treated with Δ^9-THC, with or without Cel. Data are presented as means ±SEM. *p=0.0212, ****p<0.0001 (ANOVA with Bonferroni post-hoc test, APP-TG-Veh: 25 images/5 animals, APP-TG-Cel: 25 images/5 animals, APP-TG-THC: 25 images/5 animals, APP-TG-THC: 24 images/5 animals). Scale bars: 400 μm.

Δ^9-THC alone or in combination with Cel attenuates the altered expression of synapse- and inflammation-related genes in APP-TG mice

To further investigate the mechanisms underlying the improved cognitive function in APP-TG mice treated with Δ^9-THC or the combination of Δ^9-THC and Cel, we conducted single-nucleus RNA sequencing (snRNA-seq) using the 10× Genomics Chromium platform to analyze expression of genes in the hippocampus of APP-TG mice, as previously described [41, 42]. Cell types were identified in the t-SNE plots (Fig. 5A and Suppl Fig. S1A) using canonical gene markers (Suppl Fig. S1B), including CA1 pyramidal neurons (CA1 PNs), CA3 pyramidal neurons (CA3 PNs), dentate gyrus granule cells (DG GCs), inhibitory neurons (Inh Neu), astrocytes (Ast), microglia (Mic), and oligodendrocytes (Olig).

We found significant gene up- and downregulation in hippocampal neurons, including CA1PNs, CA3PNs, and DGGCs, as well as glial cells, including Ast, Mic, and Olig, in APP-TG mice compared with WT controls (Suppl Fig. S2&3, Suppl Table S1. All supplemental tables are available for access and viewing at: https://zenodo.org/records/17488515). However, changes in expression of these genes were significantly modulated by Δ^9-THC or the combination treatment. Given the critical role of synaptic function in cognitive performance and the fact that AD at early stages is a synapse failure [38], we specifically analyzed synapse-related differentially expressed genes (DEGs). As shown in Fig. 5B~C, Suppl Fig. S4, and Suppl Table S2, synaptic genes, which are involved in synaptic organization, axon guidance, excitatory synapse formation, and spine morphology [53-56], were either up- or down-regulated in various cell types from vehicle-treated APP-TG mice. However, these alterations were significantly attenuated or restored to WT levels by Δ^9-THC or the combination treatment, with minimal effects observed following Cel treatment alone. Notably, the combination treatment resulted in a greater reversal of synaptic DEGs, particularly in neurons and astrocytes (Fig. 5B~C, Suppl Fig. S4A~G, and Suppl Table S2). Fig. 5C list representative synaptic DEGs affected across different cell types. For example, *ephb2*, a member of receptor tyrosine kinase family that plays critical roles in synaptogenesis, axon guidance, dendritic spine formation, synaptic maturation, AMPA and NMDA glutamate receptor expression and function, and long-term synaptic plasticity, is downregulated in APP-TG mice (Fig 5C). Increasing *ephb2* levels have been shown to rescue impaired synaptic plasticity in AD model animals [57]. Notably, *ephb2* is downregulated in both AD patients and APP-TG mice [48], its expression is restored by the combination treatment of Δ^9-THC and Cel. These findings suggest that the combination treatment preserves synaptic integrity and prevents synaptic and cognitive deterioration in AD. Gene Ontology (GO) enrichment analysis further supports these findings, showing that the affected DEGs are involved in synaptic organization, synaptic transmission and plasticity, and learning and memory (Fig. 5D; Supplementary Tables 3).

Neuroinflammation is considered a fundamental contributor to the pathogenesis of neurodegenerative diseases. We analyzed inflammation-related differentially expressed genes (DEGs) across all cells and within glial subsets, astrocytes, microglia, and oligodendrocytes, and found that their dysregulation in APP-TG mice was significantly reduced by Δ^9-THC, with even greater attenuation following combination treatment with Δ9-THC and celecoxib (Fig. 5E & 5F; Suppl Fig. S5; Suppl Table S4). Selected inflammation-related genes affected in different cell types are shown in Fig. 5F. GO analysis indicates that these genes are associated with immune and neuroinflammatory responses (Fig. 5D). Among them, *sharpin*, which is known to promote inflammation by enhancing the secretion of IL-1β and TNF-α in AD models, is markedly upregulated. However, this upregulated is reversed by the combination treatment (Fig. 5F).

Next, we examined the expression of AD-linked genes in APP-TG mice treated with Δ9-THC, celecoxib (Cel), or the combination. Genes up- or downregulated in vehicle-treated APP-TG mice were oppositely modulated by Δ^9-THC, with more pronounced effects under

combination treatment in CA1 PNs, CA3 PNs, DGGCs, and astrocytes (Suppl. Fig. S6; Suppl. Table S5). For example, dysregulated AD-related genes in excitatory and inhibitory neurons were reversed by Δ^9-THC, with an even greater effect from the combination (Fig. 5G). Interestingly, several AD-linked genes, *lrp1*, *apc2*, *ide*, and *kif5a*, which are involved in Aβ clearance, axonal mitochondrial transport, and AD pathogenesis [43, 58-61], were downregulated in CA1PNs and inhibitory neurons in both AD patients [43] and APP-TG mice. Their expression was restored by Δ9-THC and further enhanced by the combination treatment (Fig. 5H).

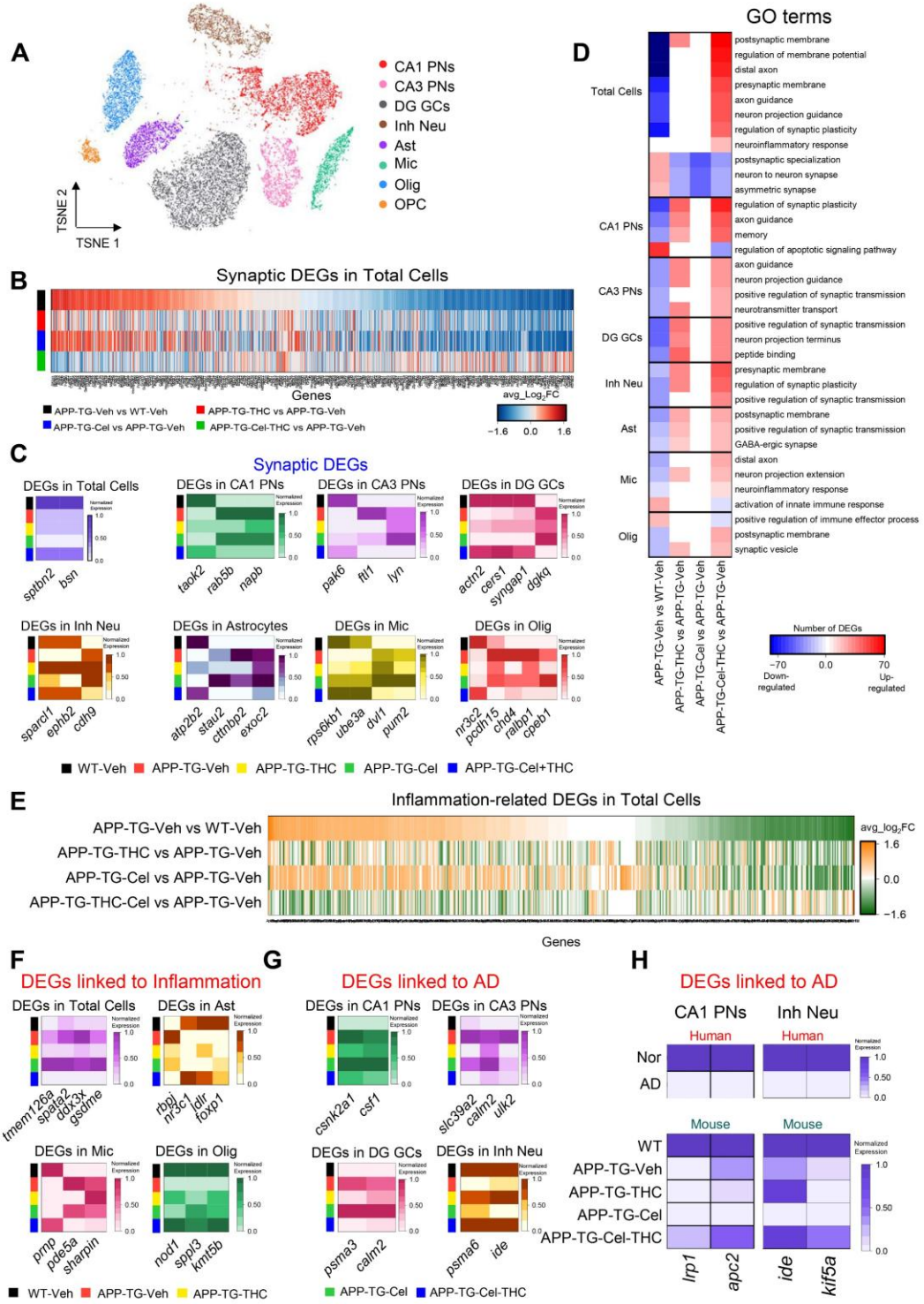

Figure 5. The combination treatment reverses altered synapse-, inflammation-, and AD-related gene expressions in the hippocampus of APP-TG mice. (A) t-Distributed Stochastic Neighbor Embedding (t-SNE) visualization of integrated nuclei from the hippocampus of WT-Veh, APP-TG-Veh, APP-TG-THC, APP-TG-Cel, and APP-TG-Cel-THC mice. Cell types include CA1 pyramidal neurons (CA1 PNs), CA3 pyramidal neurons (CA3 PNs), dentate gyrus granule cells (DG GCs), interneurons (Inh Neu), astrocytes (Ast), microglia (Mic), oligodendrocytes (Olig), and oligodendrocyte progenitor cells (OPC), **(B)** Heatmap showing the number of synapse-related differentially expressed genes (DEGs) across hippocampal cells from mice in the indicated groups. **(C)** Heatmaps displaying normalized expression levels of representative synaptic DEGs in both neurons and glial cell populations from the groups shown in **A**. **(D)** Heatmap showing the number of DEGs enriched in synapse- and inflammation-related Gene Ontology (GO) terms. **(E)** Heatmaps showing the number of inflammation-related DEGs in total hippocampal cells across the indicated groups in **A**. **(F)** Heatmaps showing normalized expression levels of representative inflammation-related DEGs in total and glial cell populations. **(G)** Heatmaps displaying representative AD-related DEGs in neuron populations. **(H)** Heatmaps showing shared DEGs in CA1 PNs and Inh Neu between human samples (from the dataset reported in reference 43) and the AD mouse model.

Since gene expression is regulated by both intracellular signaling and intercellular communication, we employed pySCENIC to predict transcription factor (TF) activity and CellChat to analyze cell-cell signaling. Following pySCENIC analysis, we examined the overlap between TF target genes and cell type-specific DEGs to identify key regulatory factors. As shown in Fig. S7A~G, activity of several key regulators related to synaptic and inflammatory functions (e.g. *esrrg* and *zfp148*) [62, 63] was higher in APP-TG mice treated with Δ^9-THC-Cel compared to vehicle-treated controls. CellChat analysis reveals significantly altered expression levels in APP-TG mice treated with vehicle, including downregulation of *slitrk3* in CA1 PNs, *ntrk2* and *psap* in DG GCs, and upregulation of *slit2* in Inh Neu (Suppl Fig. S7H). As these genes are associated with synaptic functions, their dysregulation is likely linked to impaired expression of synaptic genes observed in APP-TG mice [64-67]. While Δ^9-THC or Cel lone produced only marginal changes in these genes, the combination treatment significantly reversed these alterations (Suppl Fig. S7H). These changes of ligand/receptor levels and activity of TFs may underlie beneficial effects conferred by the combination treatment of Δ^9-THC and Cel.

Δ^9-THC alone or in combination with Cel reduces tau pathology, improves synaptic integrity and cognitive function in tau-TG mice

Given that AD features both Aβ and tau pathologies, we asked whether Δ^9-THC alone or combined with Cel could attenuate tau pathology and associated cognitive impairments. This evaluation aims to strengthen the translational relevance of our approach for potential prevention of AD by mitigating tau pathology-linked cognitive decline. To this end, we used P301S mutant human tau transgenic mice (PS19), a widely used tauopathy model [36, 37]. As shown in Fig. 6B, Δ^9-THC-induced elevation of cytokines was robustly attenuated in PS19 mice. Importantly, while Cel alone did not reduce hippocampal phosphorylated tau proteins at Thr181 (p-tau 181) and Ser202/Thr205 (AT8), nor improve learning and memory, Δ^9-THC alone or in combination with Cel significantly reduced p-tau 181 and AT8 levels and prevented cognitive decline (Fig. 6C). Importantly, Δ^9-THC, either alone or in combination with Cel prevented deterioration in spatial learning and memory retention in Tau-TG mice, as assessed by the Morris water maze (MWM) and the novel object recognition (NOR) tests (Fig. 6D~F). In addition, Δ^9-THC, alone or in combination with Cel, restored or elevated the expression of synaptic markers in the hippocampus of tauopathy model mice, including glutamate NMDA and AMPA receptor subunits and PSD95 (Fig. 6G). These results indicate that Δ^9-THC, either alone or in combination with Cel, reduces tau pathology, preserves synaptic integrity, and improves cognitive function in the tauopathy model.

DISCUSSION

Cannabis, or marijuana, has long been considered a potential therapy for AD. However, due to its complex composition, difficulties in dose control, and adverse effects associated with smoking, attention has shifted to Δ^9-THC, the primary psychoactive component of marijuana, as a potential agent for the prevention and treatment of AD. Previous studies have shown that high doses of Δ^9-THC (≥5.0 mg/kg) impair cognitive function [19], whereas low doses (≤3.0 mg/kg) improve learning and memory in aged animals [20]. These hormetic effects on neurocognitive function complicate dosage optimization and clinical implementation for preventing AD onset or slowing its progression. Consequently, few studies have evaluated Δ^9-THC as a therapeutic agent for AD, particularly, with a focus on cognitive function. Given that learning and memory impairment is the most prominent early symptom of AD, we assessed whether low dose of Δ^9-THC could prevent onset of cognitive decline in AD model animals. In this study, we provide evidence that low-dose Δ^9-THC (3.0 mg/kg in mice, equivalent to a human dose of 0.24 mg/kg) may represent an optimal intervention for preventing the development of AD, as it significantly reduces neuropathology, preserves synaptic integrity, and prevents cognitive deterioration in

two AD mouse models, one with Aβ pathology and the other with tau pathology.

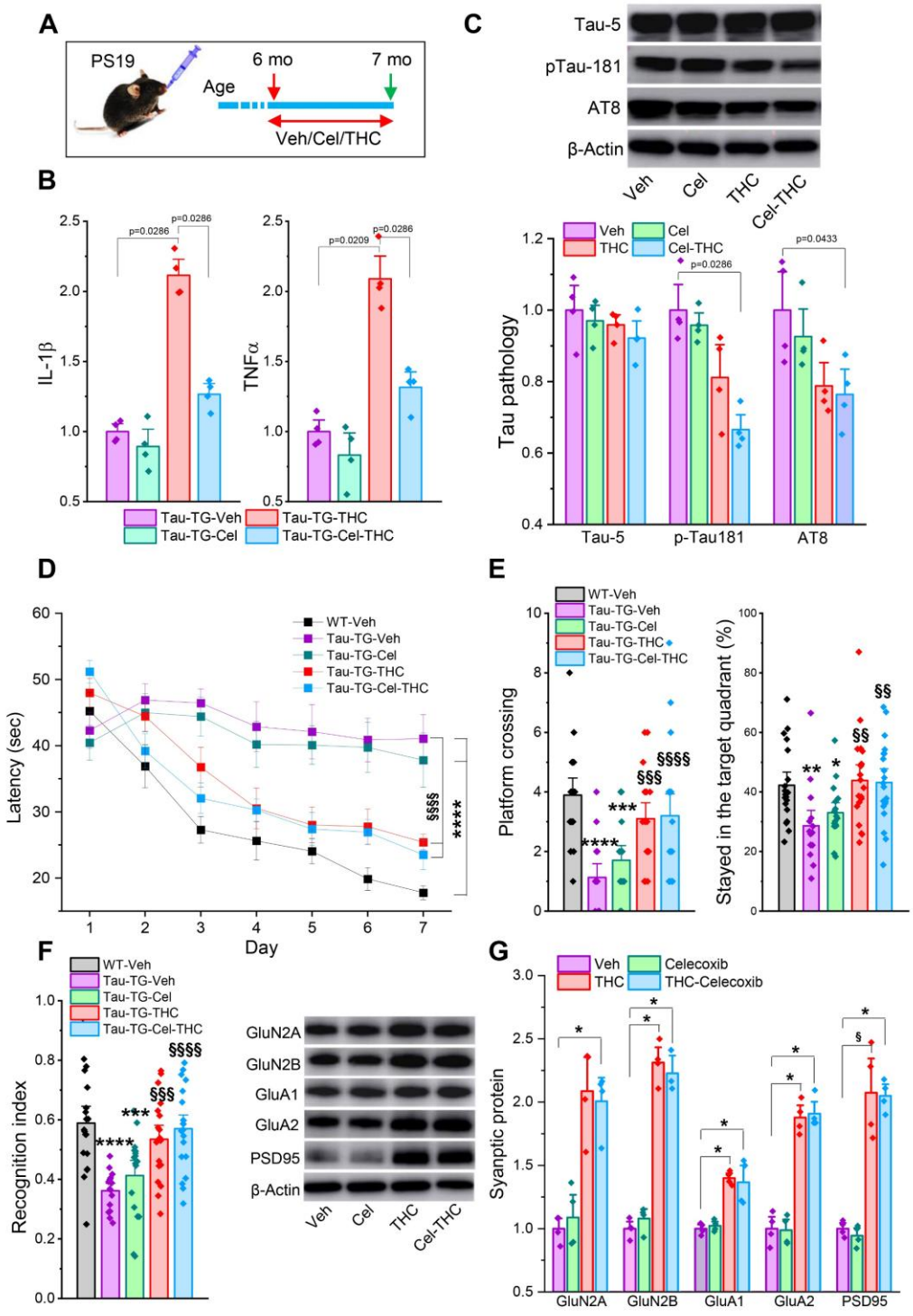

Figure 6. The combination treatment reduces tau pathology, maintains synaptic integrity, and prevents cognitive decline in tau-TG mice. (A) Schematic illustration of the experimental protocol. PS19 Tau-TG mice at six months of age received oral gavage administration of Veh, Δ^9-THC, with or without Cel. Assessments were conducted 30 days after the final dose. **(B)** ELISA analysis of cytokine levels, including IL-1β and TNFα, in hippocampal tissues of Tau-TG mice treated with Δ^9-THC, with or without Cel. Data are presented as means ±SEM (Kruskal-Wallis test followed by Dunn's post hoc test with Bonferroni correction for comparisons; n=4 animals/per group). **(C)** Immunoblot analysis of tau

pathology, including total tau (Tau-5), phosphorylated tau-Thr181 (p-Tau181), AT8 (p-Tau S202/T205), in hippocampal tissues of PS19 mice treated with Veh, Δ^9-THC, with or without Cel. Data are presented as means ±SEM (Kruskal-Wallis test followed by Dunn's post hoc test with Bonferroni correction for comparisons; n=4 animals/per group). **(D)** Spatial learning and memory retention were assessed using the Morris water maze (MWM) test. Data presented as are means ±SEM. ****P<0.0001 vs. WT-Veh, §§§§P< 0.0001vs Tau-TG-Veh (Repeated measures ANOVA with Bonferroni post hoc test, WT-Veh: n=19 animals, Tau-TG-Vel: n=15 animals, Tau-TG-Cel: n=17 animals, Tau-TG-THC: n=19 animals, Tau-TG-Cel-THC: n=20 animals). **(E)** Probe test conducted 24 hrs following 7 days of learning acquisition training. The data presented as are means ± SEM. *P=0.0386, **P=0.0038, ***P=0.0005, ****P<0.0001 vs. WT-Veh; §§P=0.0035, §§§P=0.0002,§§§§ P<0.0001 vs. Tau-TG-Veh (ANOVA with Bonferroni post-hoc test). **(F)** Novel object recognition (NOR) test. Data presented as means ±SEM. ***P=0.0002, ****P<0.0001 vs. WT-Veh; §§§P=0.0004,§§§§ P<0.0001 vs. Tau-TG-Veh (ANOVA with Bonferroni post-hoc test, WT-Veh: n=19 animals, Tau-TG-Vel: n=15 animals, Tau-TG-Cel: n=17 animals, Tau-TG-THC: n=19 animals, Tau-TG-Cel-THC: n=20 animals). **(G)** Immunoblot analysis of synaptic markers, including PSD-95 and glutamate receptor subunits (GluN1, GluN2A, GluN2B, GluA1, GluA2), in hippocampal tissues of Tau-TG mice treated with Veh, Δ^9-THC, with or without Cel. Data are presented as means ±SEM. *p=0.0286, §p=0.0433 (Kruskal-Wallis test followed by Dunn's post hoc test with Bonferroni correction for comparisons; n=4 animals/per group).

However, cannabinoids not only possess anti-inflammatory properties [1, 30], but can also activate neuroinflammatory signaling pathways [6, 31-33], indicating a dual role for Δ^9-THC in modulating inflammation-both suppressing and initiating inflammatory responses. Remarkably, Δ^9-THC has been shown to activate NF-κB and COX-2 signaling pathways, leading to increased levels of prostaglandins, cytokines, and other inflammatory mediators that contribute to Δ^9-THC-induced synaptic and cognitive impairments [6, 31-33]. To minimize potential adverse effects resulting from inducting inflammatory responses, we co-administered Δ^9-THC with the selective COX-2 inhibitor Celecoxib. Indeed, combining low-dose Δ^9-THC with Celecoxib (1.0 mg/kg) further improves spatial learning and attenuates Δ^9-THC-induced neuroinflammatory responses in AD animals. Transcriptomic analysis reveals that the altered synapse- and immune/inflammation-related DEGs observed in AD model animals, were reversed or attenuated by Δ^9-THC, with greater effects observed when combined with celecoxib. In particular, several downregulated AD-related DEGs observed in both AD patients and AD animal models were significantly reversed or attenuated by the combination treatment in AD animals. These findings suggest that the prevention of cognitive decline by the combination treatment is likely associated with the modulation of these synapse- and inflammation-related DEGs in AD animal models. Given the central role of neuroinflammation in neurodegeneration [21, 68, 69], the contribution of celecoxib to Δ^9-THC-mediated prevention of neuropathology and cognitive decline in AD model mice likely stems from its ability to suppress both pre-existing AD-related inflammation and Δ^9-THC-induced inflammatory signaling, despite the very low celecoxib dose used in this study (1.0 mg/kg).

Study rationale and limitation: The present study used a 30-day treatment paradigm as a proof-of-concept design to evaluate the efficacy and mechanisms of the Δ^9-THC and Celecoxib combination. Although this regimen was sufficient to elicit significant neuroprotective and anti-inflammatory effects, AD is a chronic condition, and future studies are needed to assess the long-term safety, sustained efficacy, and potential cumulative effects of this combination therapy.

Conclusion

AD is the most common cause of dementia in the elderly. Currently, there are no effective therapies available to prevent or treat AD or to slow its progression. Our studies provide experimental and preclinical evidence that the combination of low-dose Δ^9-THC (3.0 mg/kg) and Celecoxib (1.0 mg/kg) holds promise as an early intervention for preventing the onset of AD or treating mild cognitive impairment. This combination treatment is expected to avoid the cognitive adverse effects associated with high-dose Δ^9-THC while retaining its cognitive-enhancing benefits and minimizing Δ^9-THC-induced inflammatory responses. Especially, both Δ^9-THC (as Dronabinol and Nabilone) and Celecoxib are FDA-approved medications currently in clinical use. Therefore, this combination therapy could be rapidly advanced to clinical trials to evaluate its efficacy in preventing or delaying the onset of AD in humans.

Acknowledgements

This work was supported in part by a grant from the National Institutes of Health (R01NS076815) and by startup and endowment funds from Joe R. & Teresa Lozano Long School of Medicine at University of Texas at San Antonio Health Science Center (to C.C.). We thank the National Institute on Drug Abuse (NIDA) Drug Supply Program for providing Δ^9-THC and the NIMH Chemical Synthesis and Drug Supply Program for providing Celecoxib. We also thank Jack Hashem and Anastasia Nelson for technical support.

Data availability

Source data are provided with this paper. Additional data supporting the findings of this study are available from the corresponding authors upon request. The supplementary tables available at: https://zenodo.org/records/17488515. The codes for reproducing can be found at: https://github.com/Dexiao211/AD-THC-and-Celecoxib. The single-nucleus RNA sequencing (snRNA-seq) data have been deposited in the NCBI Gene Expression Omnibus under accession number GSE301659.

Ethics approval and consent to participate

This study was conducted on mice following a protocol approved by the Institutional Animal Care and Use Committee of the University of Texas Health Science Center at San Antonio.

Competing interests

The authors declare no conflict of interest.

Author contributions

C.C. and J.Z. conceived the project and designed the experiments; J.Z., D.Z., M.H., and M.P. performed the experiments and/or analyzed the data; C.C. supervised the work and wrote the manuscript.

Supplementary Materials

The Supplementary data can be found online at: www.aginganddisease.org/EN/10.14336/AD.2025.1206.

References

[1] Bonini SA, Premoli M, Tambaro S, Kumar A, Maccarinelli G, Memo M, et al. (2018). Cannabis sativa: A comprehensive ethnopharmacological review of a medicinal plant with a long history. J Ethnopharmacol, 227:300-315.

[2] Russo EB (2007). History of cannabis and its preparations in saga, science, and sobriquet. Chem Biodivers, 4:1614-1648.

[3] Hasan KM (2023). Cannabis Unveiled: An Exploration of Marijuana's History, Active Compounds, Effects, Benefits, and Risks on Human Health. Subst Abuse, 17:11782218231182553.

[4] Cao C, Li Y, Liu H, Bai G, Mayl J, Lin X, et al. (2014). The potential therapeutic effects of THC on Alzheimer's disease. J Alzheimers Dis, 42:973-984.

[5] Eubanks LM, Rogers CJ, Beuscher AEt, Koob GF, Olson AJ, Dickerson TJ, et al. (2006). A molecular link between the active component of marijuana and Alzheimer's disease pathology. Mol Pharm, 3:773-777.

[6] Chen R, Zhang J, Fan N, Teng ZQ, Wu Y, Yang H, et al. (2013). Delta9-THC-caused synaptic and memory impairments are mediated through COX-2 signaling. Cell, 155:1154-1165.

[7] Farkhondeh T, Khan H, Aschner M, Samini F, Pourbagher-Shahri AM, Aramjoo H, et al. (2020). Impact of Cannabis-Based Medicine on Alzheimer's Disease by Focusing on the Amyloid β-Modifications: A Systematic Study. CNS Neurol Disord Drug Targets, 19:334-343.

[8] Cohen LM, Ash E, Outen JD, Vandrey R, Amjad H, Agronin M, et al. (2024). Study rationale and baseline data for pilot trial of dronabinol adjunctive treatment of agitation in Alzheimer's dementia (THC-AD). Int Psychogeriatr, 36:1245-1250.

[9] Herrmann N, Ruthirakuhan M, Gallagher D, Verhoeff N, Kiss A, Black SE, et al. (2019). Randomized Placebo-Controlled Trial of Nabilone for Agitation in Alzheimer's Disease. Am J Geriatr Psychiatry, 27:1161-1173.

[10] Bosnjak Kuharic D, Markovic D, Brkovic T, Jeric Kegalj M, Rubic Z, Vuica Vukasovic A, et al. (2021). Cannabinoids for the treatment of dementia. Cochrane Database Syst Rev, 9:Cd012820.

[11] Bahji A, Meyyappan AC, Hawken ER (2020). Cannabinoids for the Neuropsychiatric Symptoms of Dementia: A Systematic Review and Meta-Analysis. Can J Psychiatry, 65:365-376.

[12] van den Elsen GA, Ahmed AI, Verkes RJ, Kramers C, Feuth T, Rosenberg PB, et al. (2015). Tetrahydrocannabinol for neuropsychiatric symptoms in dementia: A randomized controlled trial. Neurology, 84:2338-2346.

[13] Chen C. 2025. Chapter 27 - Endocannabinoids and Alzheimer's disease. In Handbook of Behavioral Neuroscience. O.J. Manzoni, and V. Trezza, editors: Elsevier. 451-469.

[14] Puighermanal E, Marsicano G, Busquets-Garcia A, Lutz B, Maldonado R, Ozaita A (2009). Cannabinoid modulation of hippocampal long-term memory is mediated by mTOR signaling. Nat Neurosci, 12:1152-1158.

[15] Varvel SA, Hamm RJ, Martin BR, Lichtman AH (2001). Differential effects of delta 9-THC on spatial reference and working memory in mice. Psychopharmacology (Berl), 157:142-150.

[16] Lichtman AH, Martin BR (1996). Delta 9-tetrahydrocannabinol impairs spatial memory through a cannabinoid receptor mechanism. Psychopharmacology (Berl), 126:125-131.

[17] Tinklenberg JR, Melges FT, Hollister LE, Gillespie HK (1970). Marijuana and immediate memory. Nature, 226:1171-1172.

[18] Adam KCS, Doss MK, Pabon E, Vogel EK, de Wit H (2020). Δ(9)-Tetrahydrocannabinol (THC) impairs visual working memory performance: a randomized crossover trial. Neuropsychopharmacology, 45:1807-1816.

[19] Calabrese EJ, Rubio-Casillas A (2018). Biphasic effects of THC in memory and cognition. Eur J Clin Invest, 48:e12920.

[20] Bilkei-Gorzo A, Albayram O, Draffehn A, Michel K, Piyanova A, Oppenheimer H, et al. (2017). A chronic low dose of Delta(9)-tetrahydrocannabinol (THC) restores cognitive function in old mice. Nat Med, 23:782-787.

[21] Heneka MT, Carson MJ, El Khoury J, Landreth GE, Brosseron F, Feinstein DL, et al. (2015). Neuroinflammation in Alzheimer's disease. Lancet Neurol, 14:388-405.

[22] Heppner FL, Ransohoff RM, Becher B (2015). Immune attack: the role of inflammation in Alzheimer disease. Nat Rev Neurosci, 16:358-372.

[23] Zhang W, Xiao D, Mao Q, Xia H (2023). Role of neuroinflammation in neurodegeneration development. Signal Transduct Target Ther, 8:267.

[24] Choi SH, Aid S, Caracciolo L, Minami SS, Niikura T, Matsuoka Y, et al. (2013). Cyclooxygenase-1 inhibition reduces amyloid pathology and improves memory deficits in a mouse model of Alzheimer's disease. J Neurochem, 124:59-68.

[25] Yan Q, Zhang J, Liu H, Babu-Khan S, Vassar R, Biere AL, et al. (2003). Anti-inflammatory drug therapy alters beta-amyloid processing and deposition in an animal model of Alzheimer's disease. J Neurosci, 23:7504-7509.

[26] Mhillaj E, Morgese MG, Tucci P, Furiano A, Luongo L, Bove M, et al. (2018). Celecoxib Prevents Cognitive Impairment and Neuroinflammation in Soluble Amyloid β-treated Rats. Neuroscience, 372:58-73.

[27] Lyketsos CG, Breitner JC, Green RC, Martin BK, Meinert C, Piantadosi S, et al. (2007). Naproxen and celecoxib do not prevent AD in early results from a randomized controlled trial. Neurology, 68:1800-1808.

[28] Thal LJ, Ferris SH, Kirby L, Block GA, Lines CR, Yuen E, et al. (2005). A randomized, double-blind, study of rofecoxib in patients with mild cognitive impairment. Neuropsychopharmacology, 30:1204-1215.

[29] Cole GM, Frautschy SA (2010). Mechanisms of action of non-steroidal anti-inflammatory drugs for the prevention of Alzheimer's disease. CNS Neurol Disord Drug Targets, 9:140-148.

[30] Aso E, Ferrer I (2014). Cannabinoids for treatment of Alzheimer's disease: moving toward the clinic. Front Pharmacol, 5:37.

[31] Jouroukhin Y, Zhu X, Shevelkin AV, Hasegawa Y, Abazyan B, Saito A, et al. (2019). Adolescent Δ(9)-Tetrahydrocannabinol Exposure and Astrocyte-Specific Genetic Vulnerability Converge on Nuclear Factor-κB-Cyclooxygenase-2 Signaling to Impair Memory in Adulthood. Biol Psychiatry, 85:891-903.

[32] Zamberletti E, Gabaglio M, Grilli M, Prini P, Catanese A, Pittaluga A, et al. (2016). Long-term hippocampal glutamate synapse and astrocyte dysfunctions underlying the altered phenotype induced by adolescent THC treatment in male rats. Pharmacol Res, 111:459-470.

[33] Zamberletti E, Gabaglio M, Prini P, Rubino T, Parolaro D (2015). Cortical neuroinflammation contributes to long-term cognitive dysfunctions following adolescent delta-9-tetrahydrocannabinol treatment in female rats. Eur Neuropsychopharmacol, 25:2404-2415.

[34] Oakley H, Cole SL, Logan S, Maus E, Shao P, Craft J, et al. (2006). Intraneuronal beta-amyloid aggregates, neurodegeneration, and neuron loss in transgenic mice with five familial Alzheimer's disease mutations: potential factors in amyloid plaque formation. J Neurosci, 26:10129-10140.

[35] Chen R, Zhang J, Wu Y, Wang D, Feng G, Tang YP, et al. (2012). Monoacylglycerol lipase is a therapeutic target for Alzheimer's disease. Cell Rep, 2:1329-1339.

[36] Hashem J, Hu M, Zhang J, Gao F, Chen C (2021). Inhibition of 2-Arachidonoylglycerol Metabolism Alleviates Neuropathology and Improves Cognitive Function in a Tau Mouse Model of Alzheimer's Disease. Mol Neurobiol, 58:4122-4133.

[37] Yoshiyama Y, Higuchi M, Zhang B, Huang SM, Iwata N, Saido TC, et al. (2007). Synapse loss and microglial activation precede tangles in a P301S tauopathy mouse model. Neuron, 53:337-351.

[38] Selkoe DJ (2002). Alzheimer's disease is a synaptic failure. Science, 298:789-791.

[39] Sang N, Zhang J, Marcheselli V, Bazan NG, Chen C (2005). Postsynaptically synthesized prostaglandin E2 (PGE2) modulates hippocampal synaptic transmission via a presynaptic PGE2 EP2 receptor. J Neurosci, 25:9858-9870.

[40] Zhang J, Chen C (2008). Endocannabinoid 2-arachidonoylglycerol protects neurons by limiting COX-2 elevation. J Biol Chem, 283:22601-22611.

[41] Hu M, Zhu D, Zhang J, Gao F, Hashem J, Kingsley P, et al. (2022). Enhancing endocannabinoid signalling in astrocytes promotes recovery from traumatic brain injury. Brain, 145:179-193.

[42] Zhu D, Zhang J, Hashem J, Gao F, Chen C (2023). Inhibition of 2-arachidonoylglycerol degradation enhances glial immunity by single-cell transcriptomic analysis. J Neuroinflammation, 20:17.

[43] Zhou Y, Su Y, Li S, Kennedy BC, Zhang DY, Bond AM, et al. (2022). Molecular landscapes of human hippocampal immature neurons across lifespan. Nature, 607:527-533.

[44] Jin S, Guerrero-Juarez CF, Zhang L, Chang I, Ramos R, Kuan CH, et al. (2021). Inference and analysis of cell-cell communication using CellChat. Nat Commun, 12:1088.

[45] Van de Sande B, Flerin C, Davie K, De Waegeneer M, Hulselmans G, Aibar S, et al. (2020). A scalable SCENIC workflow for single-cell gene regulatory network analysis. Nat Protoc, 15:2247-2276.

[46] Gao F, Hu M, Zhang J, Hashem J, Chen C (2022). TDP-43 drives synaptic and cognitive deterioration following traumatic brain injury. Acta Neuropathol, 144:187-210.

[47] Zhang J, Hu M, Teng Z, Tang YP, Chen C (2014). Synaptic and cognitive improvements by inhibition of 2-AG metabolism are through upregulation of microRNA-188-3p in a mouse model of Alzheimer's disease. J Neurosci, 34:14919-14933.

[48] Song Y, Hu M, Zhang J, Teng ZQ, Chen C (2019). A novel mechanism of synaptic and cognitive impairments mediated via microRNA-30b in Alzheimer's disease. EBioMedicine, 39:409-421.

[49] Antunes M, Biala G (2012). The novel object recognition memory: neurobiology, test procedure, and its modifications. Cogn Process, 13:93-110.
[50] Leger M, Quiedeville A, Bouet V, Haelewyn B, Boulouard M, Schumann-Bard P, et al. (2013). Object recognition test in mice. Nat Protoc, 8:2531-2537.
[51] Zhang J, Teng Z, Song Y, Hu M, Chen C (2015). Inhibition of monoacylglycerol lipase prevents chronic traumatic encephalopathy-like neuropathology in a mouse model of repetitive mild closed head injury. J Cereb Blood Flow Metab, 35:443-453.
[52] Sarne Y, Toledano R, Rachmany L, Sasson E, Doron R (2018). Reversal of age-related cognitive impairments in mice by an extremely low dose of tetrahydrocannabinol. Neurobiol Aging, 61:177-186.
[53] Kim H, Jeon Y, Kim S, Guo Y, Kim D, Jang G, et al. (2025). EphB2 receptor tyrosine kinase-mediated excitatory synaptic functions are negatively modulated by MDGA2. Prog Neurobiol, 250:102772.
[54] Goetze B, Tuebing F, Xie Y, Dorostkar MM, Thomas S, Pehl U, et al. (2006). The brain-specific double-stranded RNA-binding protein Staufen2 is required for dendritic spine morphogenesis. J Cell Biol, 172:221-231.
[55] Al-Ali H, Ding Y, Slepak T, Wu W, Sun Y, Martinez Y, et al. (2017). The mTOR Substrate S6 Kinase 1 (S6K1) Is a Negative Regulator of Axon Regeneration and a Potential Drug Target for Central Nervous System Injury. J Neurosci, 37:7079-7095.
[56] Ahmad-Annuar A, Ciani L, Simeonidis I, Herreros J, Fredj NB, Rosso SB, et al. (2006). Signaling across the synapse: a role for Wnt and Dishevelled in presynaptic assembly and neurotransmitter release. J Cell Biol, 174:127-139.
[57] Cisse M, Halabisky B, Harris J, Devidze N, Dubal DB, Sun B, et al. (2011). Reversing EphB2 depletion rescues cognitive functions in Alzheimer model. Nature, 469:47-52.
[58] Hares K, Miners JS, Cook AJ, Rice C, Scolding N, Love S, et al. (2017). Overexpression of Kinesin Superfamily Motor Proteins in Alzheimer's Disease. J Alzheimers Dis, 60:1511-1524.
[59] Shinohara M, Tachibana M, Kanekiyo T, Bu G (2017). Role of LRP1 in the pathogenesis of Alzheimer's disease: evidence from clinical and preclinical studies. J Lipid Res, 58:1267-1281.
[60] Zheng X, Demirci FY, Barmada MM, Richardson GA, Lopez OL, Sweet RA, et al. (2015). Genome-wide copy-number variation study of psychosis in Alzheimer's disease. Transl Psychiatry, 5:e574.
[61] Zou F, Carrasquillo MM, Pankratz VS, Belbin O, Morgan K, Allen M, et al. (2010). Gene expression levels as endophenotypes in genome-wide association studies of Alzheimer disease. Neurology, 74:480-486.
[62] Fox SN, Savage CH, Amireddy NR, McMeekin LJ, Crossman DK, Detloff PJ, et al. (2025). Estrogen-related receptor gamma is a regulator of mitochondrial, autophagy, and immediate-early gene programs in spiny projection neurons: Relevance for transcriptional changes in Huntington disease. Neurobiol Dis, 206:106818.
[63] Stevens SJ, van Essen AJ, van Ravenswaaij CM, Elias AF, Haven JA, Lelieveld SH, et al. (2016). Truncating de novo mutations in the Krüppel-type zinc-finger gene ZNF148 in patients with corpus callosum defects, developmental delay, short stature, and dysmorphisms. Genome Med, 8:131.
[64] Cove J, Morales CR, Baranes D (2006). SGP-1 increases dendritic and synaptic development dependent on synaptic activity. Neurosci Res, 56:372-385.
[65] Ke C, Gao F, Tian X, Li C, Shi D, He W, et al. (2017). Slit2/Robo1 Mediation of Synaptic Plasticity Contributes to Bone Cancer Pain. Mol Neurobiol, 54:295-307.
[66] Takahashi H, Katayama K, Sohya K, Miyamoto H, Prasad T, Matsumoto Y, et al. (2012). Selective control of inhibitory synapse development by Slitrk3-PTPδ trans-synaptic interaction. Nat Neurosci, 15:389-398, s381-382.
[67] Yoshii A, Constantine-Paton M (2010). Postsynaptic BDNF-TrkB signaling in synapse maturation, plasticity, and disease. Dev Neurobiol, 70:304-322.
[68] Kwon HS, Koh SH (2020). Neuroinflammation in neurodegenerative disorders: the roles of microglia and astrocytes. Transl Neurodegener, 9:42.
[69] Ransohoff RM (2016). How neuroinflammation contributes to neurodegeneration. Science, 353:777-783.